IEEE Access
Multidisciplinary | Rapid Review | Open Access Journal

Received 31 August 2023, accepted 25 September 2023, date of publication 29 September 2023,
date of current version 18 October 2023.

Digital Object Identifier 10.1109/ACCESS.2023.3320956

RESEARCH ARTICLE

Disturbance Observer-Based PID Control System Using DNA Strand Displacement and Its Application in Exponential Gate

WUJIE ZHANG[1] AND HUI LV[1,2]

[1]Key Laboratory of Advanced Design and Intelligent Computing, Ministry of Education, School of Software Engineering, Dalian University, Dalian, Liaoning 116622, China
[2]State Key Laboratory of Synthetical Automation for Process Industries, Northeastern University, Shenyang, Liaoning 110004, China

Corresponding author: Hui Lv (lh8481@tom.com)

This work was supported in part by the 111 Project under Grant D23006; in part by the National Natural Science Foundation of China under Grant 62272079 and Grant 61972266; in part by the Natural Science Foundation of Liaoning Province under Grant 2021-MS-344, Grant 2021-KF-11-03, and Grant 2022-KF-12-14; in part by the Scientific Research Fund of Liaoning Provincial Education Department under Grant LJKZZ20220147; in part by the Scientific Research Platform Project of Dalian University under Grant 202301YB02; in part by the State Key Laboratory of Synthetical Automation for Process Industries; in part by the State Key Laboratory of Light Alloy Casting Technology for High-End Equipment under Grant LACT-006; in part by the Postgraduate Education Reform Project of Liaoning Province under Grant LNYJG2022493; and in part by the Dalian Outstanding Young Science and Technology Talent Support Program under Grant 2022RJ08.

ABSTRACT Synthetic control circuits have demonstrated their effectiveness in molecular process control. However, current synthetic control circuits counteract the impact of disturbances by error signals. A disturbance suppression strategy that combines a disturbance observer with a controller to achieve better disturbance suppression is presented in this paper. A disturbance observer-based PID control system (DOB-PID) is implemented for the first time using chemical reaction networks (CRNs). The controller parameters are obtained using the flow direction algorithm, which significantly reduces the parameter setting time. The DOB-PID based on CRNs achieves improved disturbance suppression without affecting the setpoint tracking characteristics. To overcome the limitation of the classic disturbance observer relying on the inverse nominal model, a modified disturbance observer-based control system (MDOB) is realized using CRNs. The MDOB-PID eliminates the need for the inverse nominal model in the modeling process. Furthermore, the MDOB-PID control system is combined with a feedforward controller, resulting in a modified disturbance observer-based feedforward control system (FDOB). This system effectively decouples the set value following and disturbance suppression characteristics, simplifying the parameter tuning process. Additionally, a FDOB-PID control system is established using DNA strand displacement. The FDOB-PID control system proposed in this paper exhibits lower overshoot and better disturbance suppression compared to existing control systems. Finally, a FDOB-PID exponential gate control system is developed to suppress leakage response in calculation process. This system ensures accurate calculation results even in the presence of a leaky response in the exponential gate.

INDEX TERMS Chemical reaction networks, disturbance observation PID control, DSD reaction networks, flow direction algorithm, feedforward control.

I. INTRODUCTION

Synthetic biology [1] has gained significant clout since the turn of the twenty-first century and has been heralded as a transformative science that holds the secret to understanding life as well as the future. The primary research focus on

The associate editor coordinating the review of this manuscript and approving it for publication was Abdullah Iliyasu.

synthetic biology is now biological computing [2] in order to address the rising need for high-performance computing. Biological computing has been used in various domains, including molecular circuit operation [3], [4], [5] and molecular machine [6], [7], [8] due to its benefits of parallel operation and high compatibility.

One of the popular programming languages for molecular circuit modeling is chemical reaction networks(CRNs) [9]. Many molecular devices, including molecular transformers [10] and logic circuits [11], have been designed in recent years by researchers using CRNs. Basic chemical processes (such as catalytic reactions, degradation reactions, and annihilation events) may be easily mapped to DNA displacement reaction networks(DSD), making DNA molecules excellent building blocks of molecular devices based on CRNs [12], [13]. Currently, DSD reaction networks may be used to construct an increasing number of molecular devices based on CRNs, including PI [14], quasi-sliding mode controller [15], PID [16], 2DOF PID [17], cascade PID [18], and others.

Due to their high degree of storage and programmability, DNA molecules have been widely used in DNA computing [19], [20], [21]. The exponential gate [22] based on DNA molecules can be constructed by addition gate and multiplication gate, where the concentration of the DNA chain represents both its input and output. Exponential gates based on DNA molecules are important components of some molecular circuits [23], [24]. However, the leakage reaction can lower the concentration of the starting species, which will then result in a drop in the concentration of the products [25]. For instance, the exponential operation gate can produce inaccurate computation results due to the leakage response. The control system is typically paired with the operation gate [17], [26] to prevent the leakage reaction-related calculation result error. The outcomes indicate that the molecular control system is efficient in reducing the effects of the leakage reaction on the computation outcomes. Consequently, research on molecular controllers has gained popularity over the past several years. Oishi and Klavins [27] constructed a linear input-output system at the molecular level for the first time, proving that ideal kinetics are very similar to chemical reaction models. Yordanov et al. [14] designed proportional-integral controllers through three reaction categories of catalysis, degradation, and annihilation, and proved the possibility of using DSD to realize molecular controllers. Paulino et al. [16] developed a time-delayed first-order system using CRNs and applied a CRN-based PID controller to regulate the system. On this basis, Yuan et al. [17] proposed a 2DOF controller through the combination of a PID controller and a feedforward controller. Yuan et al. [26] proposed a CRNs-based state feedback control and Romberg observer, then completed the transformation of the space state equation into a molecular controller. Li et al. [28] built a 2DOF-IMC through CRNs, which solved the time-delay problem in the controlled object.

Research on CRN-based control systems is currently primarily concerned with exploiting error signals to reduce the impact of outside disturbances, and controller design complexity is significant. In addition to being able to successfully suppress external disturbances, the disturbance observer-based control system(DOB) [29] also allows for the easy division of its overall control structure into two control loops. The outer loop controller is independently built to provide good setpoint tracking characteristics, while the compensation of the equivalent disturbance by the inner loop disturbance observer can enhance the disturbance suppression features of the system. DOB control systems have seen significant growth in recent years across a variety of industries, including mechanical equipment [30], [31], data security [32], and engineering applications [33], among others. These applications have shown that the properties of the control system may be enhanced by the addition of disturbance observers. However, this approach has not been applied to regulate molecular processes.

Under the assumption of stability, it is usually necessary to adjust the parameters of the control system to reduce the dynamic error and shorten the steady-state duration. Traditional controller parameter adjustment typically makes use of empirical approach [22] and theoretical calculation tuning method [27]. In recent years, more and more individuals have concentrated on applying optimization algorithms to fine-tune controller settings due to the rapid growth of optimization algorithms. This is so that the optimization algorithm may avoid the time-consuming parameter computation procedure by simply requiring the matching optimization cost function. Flow Direction Algorithm(FDA) [34] is an optimization algorithm that operates on physics principles. It replicates the process of fluid particles moving continuously while looking for the best answer by constantly updating the location of the particles. Karami [34] has shown through tests that the flow direction method has a greater global search capability than the widely used optimization algorithms, and the parameter setup is easier. The flow direction technique is now being used to engineering material issues [35] and tackle machine learning [36]. The flow direction method provides several advantages in the direction of establishing parameters, as seen by its broad application potential. Therefore, this paper chooses to use the FDA to tune the controller parameters.

A first-order system with time-delay is chosen as controlled object. Then, to suppress the common disturbance problem during the chemical reaction process, the DOB-PID is adopted. First, the PID controller and disturbance observer are selected according to the controlled object, then overshoot, settling time, and rise time are selected as the control system performance indicators, and the cost function of the optimization algorithm is given. The optimal outer-loop feedback controller parameters are obtained through iteration, and then a DOB-PID control system is constructed using CRNs.

The function of the feedback controller is to track the reference point, and the disturbance observer aims at disturbance suppression. The simulation results demonstrate that the DOB-PID control system cam achieve a superior disturbance suppression effect than the single feedback loop control system. Second, a modified disturbance observer-based control system (MDOB-PID) is constructed using CRNs such that it is possible to model it without using the inverse nominal model. The outcomes of the simulation demonstrate that the MDOB can overcome the constraints of the inverse nominal model and that the parameter design is more straightforward. Third, the MDOB-PID control system is combined with a feedforward controller, resulting in a modified disturbance observer-based feedforward control system (FDOB-PID). Then, using CRNs and DSD to realize the FDOB-PID control system. The outcome demonstrates that the decoupling of two control features is accomplished and that the superior set value tracking effect and disturbance suppression effect can be produced by individually adjusting the disturbance observer and the feedforward controller. Finally, FDOB-PID suggested in this research is used to manage the leakage reaction to the calculation results. The leakage response in the CRNs-based exponential operation gate is viewed as an external disturbance. The approach suggested in this research enables the exponential operation gate to acquire the right computation result even when the leaky response occurs.

The contributions of this paper are as follows: (1) DOB-PID control system is established using CRNs. The simulation results show that the control system can suppress the disturbance better while ensuring setpoint tracking characteristics. (2) DOB-PID parameter tuning and the flow direction algorithm are merged, and the automated parameter tuning is accomplished by creating a cost function that incorporates overshoot, rising time, and settling time. (3) The MDOB-PID control system using CRNs is established, which does not depend on the inverse nominal model and does not require an external feedback control loop, which reduces the complexity of designing controller parameters. (4) The CRNs-based and DSD-based FDOB-PID control systems are constructed by combining a feedforward controller with the MDOB-PID control system. Two features of setpoint tracking and disturbance suppression may be separated by configuring the settings of the MDOB-PID and feedforward controllers independently. The control system has a smaller overshoot and a higher impact of disturbance suppression, according to simulation data. (5) Inside the framework of CRNs, exponential operation gate is built. Then, the FDOB-PID is employed to suppress the impact of leaky responses that occur inside the exponential gate.

II. DOB-PID CONTROL SYSTEM

A. THEORETICAL BASIS

In this part, the basic theory for designing DOB-PID control systems is introduced. As shown in Fig. 1, the block diagram is the result of merging a disturbance observer and a feedback loop into the DOB-PID control system. The control system design is split into two steps: first, designing the disturbance observer to calculate equivalent disturbance, then compensating at the input end; second, designing the corresponding outer loop feedback control controller to make the control system meet expectations for performance.

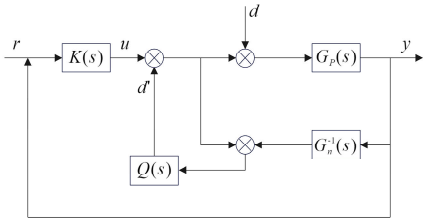

FIGURE 1. Structure of DOB-PID control system.

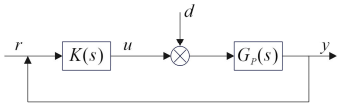

FIGURE 2. Structure of PID control system.

According to Fig. 1, $G_p(s)$ is the controlled object, $K(s)$ represents the PID controller, $G_n^{-1}(s)$ is the inverse nominal model, $Q(s)$ is the disturbance observer, the control output signal, setpoint signal, disturbance signal, equivalent disturbance signal, and output signal are marked as u, r, d, d', and y, respectively.

It can be obtained from Fig. 1 that two transfer functions of the close-loop are

$$G_{ry} = \frac{G_p(s)G_n(s)K(s)}{G_n(s)[1 + K(s)G_p(s)] + [G_p(s) - G_n(s)]Q(s)} \tag{1}$$

$$G_{dy} = \frac{G_p(s)G_n(s)[1 - Q(s)]}{G_n(s)[1 + K(s)G_p(s)] + [G_p(s) - G_n(s)]Q(s)} \tag{2}$$

where (1) is from the setpoint input signal r to the output signal y, while (2) is from the disturbance signal d to the output signal y.

From (1) and (2), it can be seen that when the nominal model is accurate, that is, $G_p(s) = G_n(s)$

$$G_{ry} = \frac{G_p(s)K(s)}{1 + K(s)G_p(s)} \tag{3}$$

$$G_{dy} = \frac{G_p(s)[1 - Q(s)]}{1 + K(s)G_p(s)} \tag{4}$$

Remark 1: It can be obtained from Fig. 2 that two transfer functions of the close-loop are

$$G_{ry} = \frac{G_p(s)K(s)}{1 + K(s)G_p(s)} \tag{5}$$

$$G_{dy} = \frac{G_p(s)}{1 + K(s)G_p(s)} \tag{6}$$

It is well known that the disturbance suppression characteristic of a control system is determined by transfer function

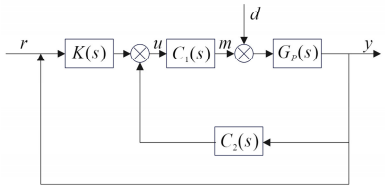

FIGURE 3. Block diagram of DOB-PID control system.

G_{dy}. The closer G_{dy} is to 0, the more effective the control system is in suppressing disturbances. At this time, comparing G_{dy} in (3)(4) of the DOB-PID control system and that in (5)(6) of the single feedback loop control system, it can be seen that when the setpoint tracking characteristics are consistent, G_{dy} in (4) is closer to 0. Therefore, the DOB-PID control system is more effective in disturbance suppression.

The transfer function from control output signal u to system output signal y is simplified as follow:

$$G_{uy} = \frac{G_p(s)G_n(s)}{G_n(s) + (G_p(s) - G_n(s))Q(s)} = \frac{\frac{G_p(s)}{1-Q(s)}}{1 + \frac{Q(s)}{G_n(s)}\frac{G_p(s)}{1-Q(s)}} \tag{7}$$

According to the transfer function (7), the structure in Fig. 2 can be transformed into Fig. 3.

According to Fig. 3, $K(s)$ is the feedback controller, $C_1(s)$ and $C_2(s)$ are the equivalent controllers, which have the following forms, respectively.

$$K(s) = K_P + \frac{K_I}{s} + K_D s \tag{8}$$

$$C_1(s) = \frac{1}{1 - Q(s)} \tag{9}$$

$$C_2(s) = \frac{Q(s)}{G_n(s)} \tag{10}$$

where $Q(s)$ is depicted in (11)

$$Q(s) = \frac{1}{\lambda s + 1} \tag{11}$$

Remark 2: In this part, the basic theory for designing DOB-PID control systems is introduced. The control system design process is streamlined by splitting the control system into two control loops. Then, comparing the transfer function of DOB-PID control system with that of the single feedback loop control system, it is found that the DOB-PID control system has a better disturbance suppression effect.

B. TUNING THE DOB-PID PARAMETERS BY FLOW DIREACTION ALGORITHM

In order to make the DOB-PID control system stable with a smaller steady-state error and a shorter stable time, tuning the parameters of the control system is deemed necessary. In view of the fact that the flow direction algorithm(FDA) has certain advantages in parameter tuning, such as faster tending to the global optimum and fewer parameter settings, the FDA is chosen to tune the DOB-PID control system parameters. The process can be divided into five steps, as follows:

Step **1**. The goal of optimization is to discover a set of DOB-PID parameters that minimize the cost function. The cost function is defined specifically as:

$$fobj = \omega_1 * (mp)^2 + \omega_2 * (tr)^2 + \omega_3 * (ts)^2 \tag{12}$$

where mp is overshoot, ω_1 is overshoot weight, tr is rise time, ω_2 is rise time weight, ts is settling time, and ω_3 is settling time weight. Since mp is the first performance index, choose $\omega_1 \gg \omega_2, \omega_3$. The mp, tr, and ts of the control system corresponding to this set of parameters are all inversely proportional to the cost function.

Step **2**. Initialization. Initializing the number of search points α. Then setting the search point as follow:

$$x = \begin{bmatrix} k_P^1 & k_I^1 & k_D^1 & \lambda^1 \\ k_P^2 & k_I^2 & k_D^2 & \lambda^2 \\ \cdots & \cdots & \cdots & \cdots \\ k_P^\alpha & k_I^\alpha & k_D^\alpha & \lambda^\alpha \end{bmatrix} \tag{13}$$

where k_P, k_I, and k_D are PID parameters, λ is a disturbance observer parameter. These search points represent different DOB-PID parameters. Then setting the upper limit of iterations as n, the initial search point coordinates x_i is a random coordinate within the search range, and the flow velocity is v.

Step **3**. Calculating the cost function. Assigning the search point to the DOB-PID model and returning the mp, tr, and ts required by the cost function, then calculating the cost function of the search point in accordance with (12).

Step **4**. Updating search point position and flow direction. According to the flow update strategy of FDA, updating the locations of the search points and flow directions. The historical optimal search point is found by comparing the cost function. Then calculating the vector information between the current search point and the historical optimal search point. The following actions are detailed.

Action **1**. Comparing the cost function of the neighbor search points to the present search point. Equation (14) is applied when $fobj(x(i)) > fobj(x(j))$; otherwise, (16) is applied, where $x(i)$ is the present search point, $x(j)$ represents the neighbor search point, and $fobj(x(i))$ is the cost function of $x(i)$.

Action **2**. Executing the following calculation after designating the neighbor search point as the new optimal search point.

$$new\_x_i = x_i + v * \frac{x(i) - x(j)}{\|x(i) - x(j)\|} \tag{14}$$

where the update equation for the flow rate v is

$$v = rand * \frac{fobj(x(i)) - fobj(x(j))}{\|x(i) - x(j)\|} \tag{15}$$

where $rand$ is random numbers to generate different solutions and increase global search.

Action **3**. Another search point is chosen at random if the cost functions of all neighboring search points are higher than

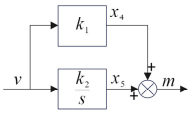

FIGURE 4. The relationship among the reactant species used to implement the controller $C_1(s)$

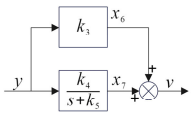

FIGURE 5. The relationship among the reactant species used to implement the controller $C_2(s)$.

that of the present search point. Then moving the search point toward the random search point, when $fobj(x(r)) < fobj(x(i))$. Otherwise, moving the search point along the direction of the optimal search point.

$$new\_x_i = \begin{cases} x_i + rand * \dfrac{x(r) - x(i)}{\|x(r) - x(i)\|}, \\ \qquad fobj(x(r)) < fobj(x(i)) \\ x_i + rand * \dfrac{best\_x(i) - x(i)}{\|best\_x(i) - x(i)\|}, \\ \qquad fobj(x(r)) > fobj(x(i)) \end{cases} \tag{16}$$

where $x(r)$ is the random search point, $best\_x(i)$ is the historical optimal search point.

Step **5**. Verifying if the upper limit of iterations has been reached. If the termination conditions are met, the current optimal PID parameters will be output; otherwise, step **3** is repeated.

Remark 3: In this part, the process of tuning the four parameters in DOB-PID using the FDA is introduced. The control system can get a reduced overshoot and a quicker stabilization time via parameter tuning. Subsequent control system parameters are all determined by the FDA, and only the search point dimension in step **2** needs to be changed. The method in this paper saves a significant amount of computation time when compared to earlier empirical methods and internal model methods.

C. CRNS-BASED DOB-PID CONTROL SYSTEM

In order to make $K(s)$, $C_1(s)$, and $C_2(s)$ more suitable for the implementation of CRNs, they are approximated as follows:

$$K(s) = K_P + \frac{K_I}{s} + K_D s = k_6 + \frac{k_7}{s} - \frac{k_8}{s + k_9} \tag{17}$$

$$C_1(s) = \frac{1}{1 - Q_A(s)} = 1 + \frac{1}{\lambda_A s} = k_1 + \frac{k_2}{s} \tag{18}$$

$$C_2(s) = \frac{Q_B(s)}{G_n(s)} = \frac{Ts + 1}{\lambda_B s + 1} = k_3 + \frac{k_4}{s + k_5} \tag{19}$$

Equations (18)(19) are obtained by combining and approximating (9)-(11), and (17) is obtained by approximating (8),where $k_1 = 1, k_2 = \frac{1}{\lambda}, k_3 = \frac{T}{\lambda}, k_4 = \frac{\lambda - T}{\lambda^2}, k_5 = \frac{1}{\lambda}$, $k_6 = k_P + \frac{k_D}{\tau}, k_7 = k_I, k_8 = \frac{4k_D}{\tau^2}, k_9 = \frac{2}{\tau}$. The control

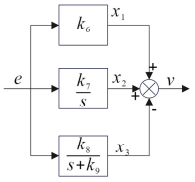

FIGURE 6. The relationship among the reactant species used to implement the controller $K(s)$.

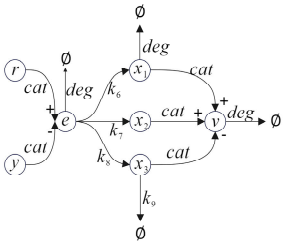

FIGURE 7. Visual depiction of CRNs for $K(s)$ (20)-(24).

structures of the controllers $K(s)$, $C_1(s)$, and $C_2(s)$ can be determined from (17)-(19) and are seen in Fig. **4**, Fig. **5**, and Fig. **6**, respectively.

According to (17)-(19), the CRNs of DOB-PID can be obtained as follows:

$$R^{\pm} \overset{cat}{\to} R^{\pm} + E^{\pm}, Y^{\pm} \overset{cat}{\to} Y^{\pm} + E^{\mp}, E^{\pm} \overset{deg}{\to} \phi, E^{+} + E^{-} \overset{ann}{\to} \phi \tag{20}$$

$$E^{\pm} \overset{k_6}{\to} E^{\pm} + X_1^{\pm}, X_1^{\pm} \overset{deg}{\to} \phi, X_1^{+} + X_1^{-} \overset{ann}{\to} \phi \tag{21}$$

$$E^{\pm} \overset{k_7}{\to} E^{\pm} + X_2^{\pm}, X_2^{+} + X_2^{-} \overset{ann}{\to} \phi \tag{22}$$

$$E^{\pm} \overset{k_8}{\to} E^{\pm} + X_3^{\pm}, X_3^{\pm} \overset{k_9}{\to} \phi, X_3^{+} + X_3^{-} \overset{ann}{\to} \phi \tag{23}$$

$$X_1^{\pm} \overset{cat}{\to} X_1^{\pm} + V^{\pm}, X_2^{\pm} \overset{cat}{\to} X_2^{\pm} + V^{\pm}, X_3^{\pm} \overset{cat}{\to} X_3^{\pm} + V^{\mp} \tag{24}$$

The feedback controller $K(s)$ shown in Fig. **6** is established by (20)-(24). The tracking error signal $e = r - y$ is generated by (20). The integral element $x_1 = k_6 e$, the integral element x'', and the differential element x'' are expressed in (21)-(23). The summing process of x_1, x_2, and x_3 is expressed by the (24). Visual depiction of (20)-(24) is shown in Fig. **7**.

$$Q^{\pm} \overset{cat}{\to} Q^{\pm} + V^{\pm}, V^{+} + V^{-} \overset{ann}{\to} \phi \tag{25}$$

$$V^{\pm} \overset{k_1}{\to} V^{\pm} + X_4^{\pm}, X_4^{\pm} \overset{deg}{\to} \phi, X_4^{+} + X_4^{-} \overset{ann}{\to} \phi \tag{26}$$

$$V^{\pm} \overset{k_2}{\to} V^{\pm} + X_5^{\pm}, X_5^{+} + X_5^{-} \overset{ann}{\to} \phi \tag{27}$$

$$X_4^{\pm} \overset{cat}{\to} X_4^{\pm} + M^{\pm}, X_5^{\pm} \overset{cat}{\to} X_5^{\pm} + M^{\pm}, M^{\pm} \overset{ann}{\to} \phi \tag{28}$$

$$Y^{\pm} \overset{k_3}{\to} Y^{\pm} + X_6^{\pm}, X_6^{\pm} \overset{deg}{\to} \phi, X_6^{+} + X_6^{-} \overset{ann}{\to} \phi \tag{29}$$

$$Y^{\pm} \overset{k_4}{\to} Y^{\pm} + X_7^{\pm}, X_7^{\pm} \overset{k_5}{\to} \phi, X_7^{+} + X_7^{-} \overset{ann}{\to} \phi \tag{30}$$

$$X_6^{\pm} \overset{cat}{\to} X_6^{\pm} + Q^{\pm}, X_7^{\pm} \overset{cat}{\to} X_7^{\pm} + Q^{\pm}, Q^{\pm} \overset{deg}{\to} \phi \tag{31}$$

The controller $C_1(s)$ shown in Fig. **4** is established by (25)-(28). The controller $C_2(s)$ shown in Fig. **5** is established by (29)-(31). The disturbance compensation signal $\delta = v - d''$

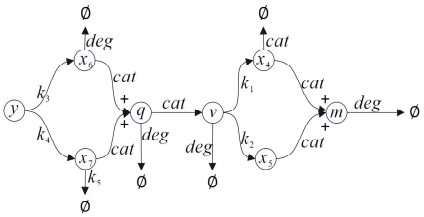

FIGURE 8. Visual depiction of CRNs for $C_1(s)$ and $C_2(s)$ (25)-(31).

TABLE 1. Parameters of controlled object $G_p(s)$.

Controlled object $G_p(s)$	
$\theta = 10$	$g_1 = 0.002$
$K = 1$	$g_2 = 0.002$
$T = 500$	$g_3 = 0.4$
$cat = 1$	$g_4 = 0.2$
$deg = 1$	
$ann = 1$	

TABLE 2. Parameters of DOB-PID and corresponding reaction rates.

Parameters of DOB-PID	Reaction rates
$k_P = 9.68$	$k_1 = 11.68$
$k_I = 0.028$	$k_2 = 0.028$
$k_D = 100.44$	$k_3 = 0.04$
$\lambda = 150.18$	$k_4 = 0.02$
	$k = 0.00667$

is generated by (25). The integral element $x_4 = k_1\delta$ and the integral element x'' are expressed in (26)-(27). The summing process of x_4 and x_5 is expressed by (28). The integral element $x_6 = k_3 e$ and the integral element x'' are expressed in (29)-(30). The summing process of x_6 and x_7 is expressed by (31). Visual depiction of (25)-(31) is shown in Fig. **8**.

The kinetic equations of the reactant species in (20)-(31) can be represented by the following equations:

$$\dot{e}^{\pm} = cat * r^{\pm} + cat * y^{\mp} - deg * e^{\pm} - ann * e^{+}e^{-} \quad (32)$$
$$\dot{x}_1^{\pm} = k_6 * e^{\pm} - deg * x_1^{\pm} - ann * x_1^{+}x_1^{-} \quad (33)$$
$$\dot{x}_2^{\pm} = k_7 * e^{\pm} - ann * x_2^{+}x_2^{-} \quad (34)$$
$$\dot{x}_3^{\pm} = k_8 * e^{\pm} - k_9 * x_3^{\pm} - ann * x_3^{+}x_3^{-} \quad (35)$$
$$\dot{\delta}^{\pm} = cat * v^{\pm} + deg * d^{\mp} - deg * \delta^{\pm} - ann * \delta^{+}\delta^{-} \quad (36)$$
$$\dot{x}_4^{\pm} = k_1 * \delta^{\pm} - deg * x_4^{\pm} - ann * x_4^{+}x_4^{-} \quad (37)$$
$$\dot{x}_5^{\pm} = k_2 * \delta^{\pm} - deg * x_5^{\pm} - ann * x_5^{+}x_5^{-} \quad (38)$$
$$\dot{x}_6^{\pm} = k_3 * y^{\pm} - deg * x_6^{\pm} - ann * x_6^{+}x_6^{-} \quad (39)$$
$$\dot{x}_7^{\pm} = k_4 * y^{\pm} - k_5 * x_7^{\pm} - ann * x_7^{+}x_7^{-} \quad (40)$$

Remark 4: This section gives the chemical reaction networks used to realize DOB-PID. By utilizing the CRNs

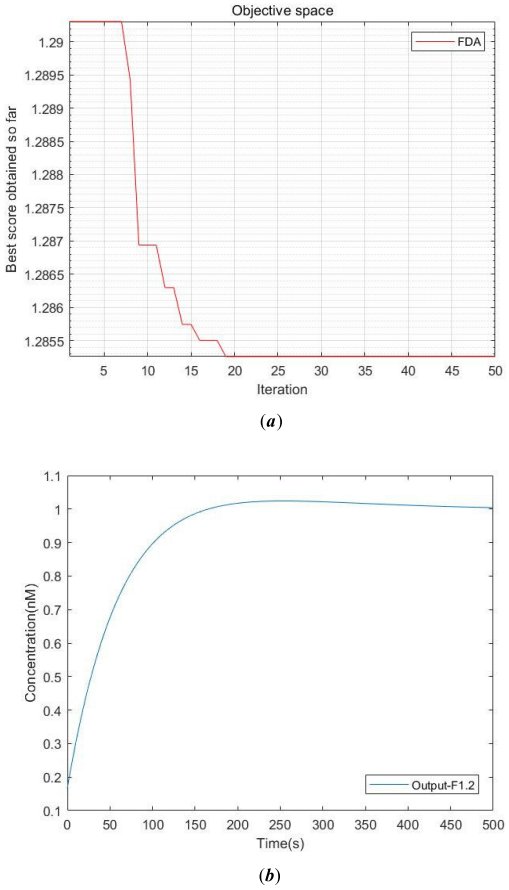

FIGURE 9. (*a*) The process of tuning controller parameters in DOB-PID by FDA (*b*) Step response of DOB-PID control system.

TABLE 3. Step response performance of PID and DOB-PID based on CRNs, when $r(t) = 1(t)$, $d(t) = 0(t)$.

Control system	$r(t) = 1(t)$, $d(t) = 0(t)$		
	Rise time	Settling time	Overshoot
PID[16]	92.55s	433.34s	2.37%
DOB-PID	**86.43s**	**416.62s**	**2.27%**

TABLE 4. Step response performance of PID and DOB-PID based on CRNs, when $r(t) = 1(t)$, $d(t) = 1(t)$.

Control system	$r(t) = 1(t)$, $d(t) = 1(t)$		
	Rise time	Settling time	Overshoot
PID[16]	73.04s	754.63s	8.21%
DOB-PID	**71.59s**	**303.59s**	**2.54%**

(20)-(31) provided in this section, it is possible to carry out the simulation of the CRNs-based DOB-PID control system.

D. CRNS-BASED CONTROLLED OBJECT

The controlled object for this paper is a first-order system with time-delay $G_p(s) = \frac{K}{Ts+1}e^{-\theta s}$. Then the time-delay term $e^{-\theta s}$ in the object $G_p(s)$ is approximated utilizing the first-order Padé approximation. As a result, the controlled plant is

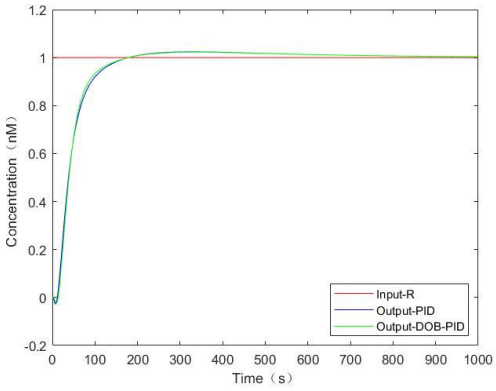

(a)

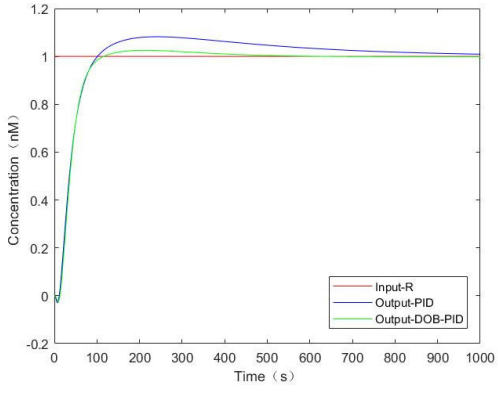

(b)

FIGURE 10. Step response curve of PID [16] and DOB-PID based on CRNs (*a*) when $r(t) = 1(t)$, $d(t) = 0(t)$ (*b*) when $r(t) = 1(t)$, $d(t) = 1(t)$.

rewritten as:

$$G_P(s) = \frac{K}{Ts+1}e^{-\theta s} = \frac{K}{Ts+1}\frac{2-\theta s}{2+\theta s} = \frac{g_1}{s+g_2}\left(\frac{g_3}{s+g_4} - 1\right) \tag{41}$$

where $g_1 = \frac{K}{T}$, $g_2 = \frac{1}{T}$, $g_3 = \frac{4}{\theta}$, and $g_4 = \frac{2}{\theta}$. According to (41), the CRNs of the object $G_p(s)$ can be obtained in (42)-(44).

$$M^{\pm} \xrightarrow{g_1} M^{\pm} + P_1^{\pm}, P_1^{\pm} \xrightarrow{g_2} \phi, P_1^{+} + P_1^{-} \xrightarrow{1} \phi \tag{42}$$

$$P_1^{\pm} \xrightarrow{g_3} P_1^{\pm} + P_2^{\pm}, P_2^{\pm} \xrightarrow{g_4} \phi, P_2^{+} + P_2^{-} \xrightarrow{1} \phi \tag{43}$$

$$P_1^{\pm} \xrightarrow{1} P_1^{\pm} + Y^{\mp}, P_2^{\pm} \xrightarrow{1} P_2^{\pm} + Y^{\pm}, Y^{\pm} \xrightarrow{g_4} \phi, Y^{+} + Y^{-} \xrightarrow{1} \phi \tag{44}$$

The kinetic equations of the reactant species in (42)-(44) can be represented by the following equations:

$$\dot{P}_1^{\pm} = g_1 * M^{\pm} - g_2 * P_1^{\pm} - ann * P_1^{+}P_1^{-} \tag{45}$$

$$\dot{P}_2^{\pm} = g_3 * P_1^{\pm} - g_4 * P_2^{\pm} - ann * P_2^{+}P_2^{-} \tag{46}$$

$$\dot{Y}^{\pm} = cat * P_1^{\mp} + cat * P_2^{\pm} - deg * Y^{\pm} - ann * Y^{+}Y^{-} \tag{47}$$

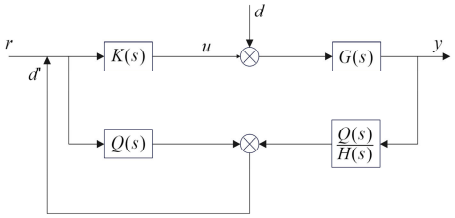

FIGURE 11. MDOB-PID control system.

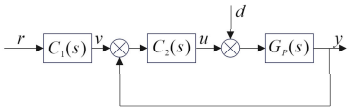

FIGURE 12. MDOB-PID control system.

Remark 5: Since first-order systems can better represent molecular processes and are easier to implement and analyze, in the analysis and design of molecular processes, higher-order systems are often approximated to first-order systems by the model step-down method as follows:

$$G_p(s) = \frac{K}{Ts^2+s+1}e^{-\theta s} \approx \frac{K}{Ts+1}\frac{1}{s+1}e^{-\theta s} = G_{p1}(s)G_{p2}(s) \tag{48}$$

where $G_{p1}(s) = \frac{K}{Ts+1}e^{-\boldsymbol{\theta s}}$ and $G_{p2}(s) = \frac{1}{s+1}$.

E. SIMULATION OF CRNS-BASED DOB-PID CONTROL SYSTEM

In this subsection, the step response of CRNs-based PID [16] and CRNs-based DOB-PID are compared. The parameters of the object $G_p(s)$ of (41) are shown in Table **1**.

The four parameters (k_P, k_I, k_D, and λ) of the DOB-PID of (17)-(19) must be tuned for the sake of improving the control performance of the DOB-PID control system.

The parameter optimization process of DOB-PID and the step response after optimization are shown in Fig. **9**. According to the optimization results of the FDA, the optimal control system parameters can be obtained as $k_P = 9.68$, $k_I = 0.028$, $k_D = 100.44$, and $\lambda = 150.18$.

The reaction rates of CRNs in Table **2** can be obtained by (17)-(19).

Through Visual DSD for simulation, the step response curves for PID [16] and DOB-PID are shown in Fig. **10**, where Output-PID represents the step response of PID [16] and Output-DOB-PID represents the step response of DOB-PID.

According to Fig. **10**, since the addition of the disturbance observer introduces an additional integral link, when there is no disturbance in the system, the DOB-PID control system demonstrates a superior tracking effect of the setpoint compared to the single feedback loop control system. When there is a disturbance $d(t) = 1(t)$, the DOB-PID control system exhibits a significantly superior ability to suppress disturbances compared to its counterpart, PID [16]. Additionally,

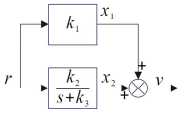

FIGURE 13. The relationship among the reactant species used to implement the controller $C_1(s)$.

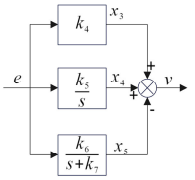

FIGURE 14. The relationship among the reactant species used to implement the controller $C_2(s)$.

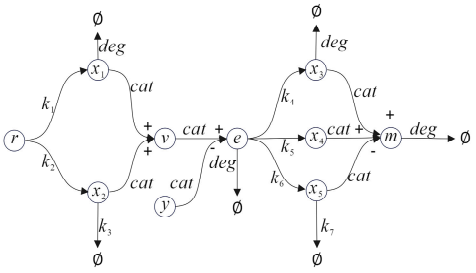

FIGURE 15. Visual depiction of CRNs for MDOB-PID (59)-(66).

PID [16] has produced a larger overshoot, and the settling time is obviously increased, while the DOB-PID control system does not produce a large amount of overshoot, and the settling time is shorter. The above outcomes prove that the DOB-PID control system can meet higher disturbance suppression requirements without affecting setpoint tracking. The respective data in detail are displayed in Table 3 and Table 4.

Remark 6: In this part, a simulation comparison between the single feedback loop control system [16] and the CRNs-based DOB-PID control system is provided. It is demonstrated that the molecular control system can exhibit an enhanced ability to suppress disturbances with the addition of a disturbance observer. However, it is discovered that the DOB-PID control system has several limitations, such as its reliance on the inverse nominal model. To overcome this limitation, the expectation model is used instead of the inverse nominal model in the next section of this paper. The modified control system will no longer depend on the inverse nominal model.

III. MODIFIED OBSERVER-BASED PID CONTROL SYSTEM

A. THEORETICAL BASIS

The classic disturbance observer relies on the inverse nominal model. The modified disturbance observer-based PID control system (MDOB-PID) is suggested to get rid of this restriction, whose basic block diagram is shown in Fig. 11.

TABLE 5. Parameters of $G_P(s)$.

Controlled object $G_p(s)$	
$\theta = 1\times10^5$	$g_1 = 0.000005$
$K = 1$	$g_2 = 0.000005$
$T = 2\times10^5$	$g_3 = 0.00004$
$cat = 1$	$g_4 = 0.00002$
$deg = 1$	
$ann = 1$	

TABLE 6. Parameters of the MDOB-PID control system.

$\tau_q = 4\times10^5$	$\tau_q = 2\times10^5$	$\tau_q = 10^5$
$k_1 = 2$	$k_1 = 1$	$k_1 = 0.5$
$k_2 = 0.000005$	$k_2 = 0.000005$	$k_2 = 0.0000025$
$k_3 = 0.000005$	$k_3 = 0.000005$	$k_3 = 0.000005$
$k_4 = 0.5$	$k_4 = 1$	$k_4 = 2$
$k_5 = 0.0000025$	$k_5 = 0.000005$	$k_5 = 0.00001$

According to Fig. 11, $K(s)$ is the pre-compensator, $Q(s)$ is the filter, $H(s)$ is the expectation model, r represents the input signal, d is the external disturbance signal, u is the control output signal, y is the system output signal.

As shown in Fig. 11, by including an adjustable expectation model $H(s)$, the MDOB-PID avoids the dependence of the classical DOB-PID on the inverse nominal model. The MDOB-PID control system can be seen as the DOB-PID control system without feedback controller when $K(s) = 1$ and $H(s) = G_n(s)$, which lowers the total control system design complexity. Two transfer functions of the close-loop are:

$$G_{ry} = \frac{G(s)H(s)K(s)}{H(s)\left[1 - Q(s)\right] + G(s)Q(s)K(s)} \tag{49}$$

$$G_{dy} = \frac{G(s)H(s)[1 - Q(s)]}{H(s)[1 - Q(s)] + G(s)Q(s)K(s)} \tag{50}$$

where (49) is from input signal r to output signal y, while (50) is from disturbance signal d to output signal y. Meanwhile, $K(s)$, $Q(s)$, and $H(s)$ have the following forms

$$K(s) = K_{PD} + \lambda s \tag{51}$$

$$Q(s) = \frac{1}{\tau_q s + 1} \tag{52}$$

$$H(s) = \frac{1}{\tau_c s + 1} \tag{53}$$

where K_{PD} and λ are parameters of the pre-compensator, τ_q is parameter of the filter, τ_c is parameter of the expectation model. To make $G(s)K(s) \approx H(s)$ as much as possible, let $K_{PD} = \frac{T}{K\tau_c}$ (T and K are parameters of the controlled plant).

TABLE 7. Step response performance of MDOB-PID based on CRNs, when $r(t) = 1(t)$, $d(t) = 0(t)$.

τ_q	$r(t)=1(t)\,,\ d(t)=0(t)$		
	Rise time	Settling time	Overshoot
$\tau_q = 4\times10^5$	389546s	1073021s	5.00%
$\tau_q = 2\times10^5$	325079s	610771s	3.07%
$\tau_q = 10^5$	246179s	695519s	1.80%

TABLE 8. Step response performance of MDOB-PID based on CRNs, when $r(t) = 1(t)$, $d(t) = 2(t)$.

τ_q	$r(t)=1(t)\,,\ d(t)=2(t)$		
	Rise time	Settling time	Overshoot
$\tau_q = 4\times10^5$	267235s	2861744s	33.30%
$\tau_q = 2\times10^5$	253020s	1573445s	27.05%
$\tau_q = 10^5$	231319s	832834s	20.25%

Transfer function (48) is simplified as follow:

$$G_{ry} = \frac{\frac{Q(s)G(s)K(s)}{H(s)[1-Q(s)]}}{1+\frac{Q(s)G(s)K(s)}{H(s)[1-Q(s)]}} * \frac{H(s)}{Q(s)} \tag{54}$$

According to the transfer function (54), a transformed structure of the MDOB-PID control system presented in Fig. 12.

According to Fig. 12, $C_1(s)$ and $C_2(s)$ are the equivalent controllers, which have the following forms, respectively.

$$C_{1(s)} = \frac{H(s)}{Q(s)} = \frac{\tau_q s+1}{\tau_c s+1} \tag{55}$$

$$C_{2(s)} = \frac{Q(s)K(s)}{H(s)[1-Q(s)]} = k_P + \frac{k_I}{s} + k_D s \tag{56}$$

where $k_P = \frac{T}{K\tau_q} + \frac{\lambda}{\tau_q}$, $k_I = \frac{T}{K\tau_q\tau_c}$, $k_D = \frac{\lambda\tau_c}{\tau_q}$.

Remark 7: In this part, the basic theory for designing MDOB-PID control system is introduced. The modified control system gets rid of the limitation of the classical DOB-PID control system, which relies on the inverse nominal model, by introducing an adjustable expectation model.

B. CRNS-BASED MDOB-PID CONTROL SYSTEM

In order to make $C_1(s)$ and $C_2(s)$ more suitable for the implementation of CRNs, they are approximated as follows:

$$C_1(s) = \frac{H(s)}{Q(s)} = \frac{\tau_q s+1}{\tau_c s+1} = k_1 + \frac{k_2}{s+k_3} \tag{57}$$

$$\begin{aligned} C_2(s) &= \frac{Q(s)K(s)}{H(s)[1-Q(s)]} = k_P + \frac{k_I}{s} + k_D s \\ &= k_4 + \frac{k_5}{s} - \frac{k_6}{s+k_7} \end{aligned} \tag{58}$$

where $k_1 = \frac{\tau_q}{\tau_c}$, $k_2 = \frac{\tau_c-\tau_q}{\tau_c^2}$, $k_3 = \frac{1}{\tau_c}$, $k_4 = k_P + \frac{2k_D}{\tau}$, $k_5 = k_I$, $k_6 = \frac{4k_D}{\tau^2}$,and $k_7 = \frac{2}{\tau}$.

The control structures of the controllers $C_1(s)$, and $C_2(s)$ can be determined from (57)-(58) and are seen in Fig. 13 and Fig. 14, respectively, whose CRNs are as follows:

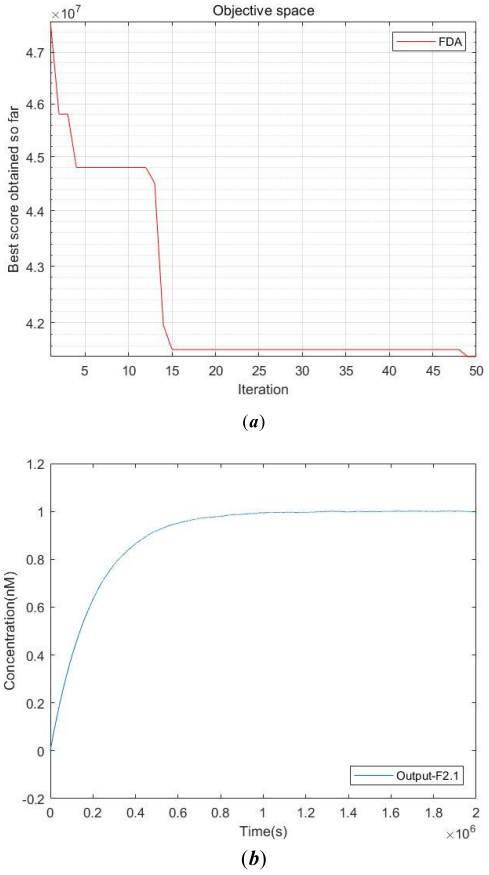

FIGURE 16. (a) The process of tuning controller parameters in MDOB-PID by FDA (b) Step response of MDOB-PID control system.

$$R^{\pm} \xrightarrow{k_1} R^{\pm} + X_1^{\pm}, X_1^{\pm} \xrightarrow{deg} \phi, X_1^{+} + X_1^{-} \xrightarrow{ann} \phi \tag{59}$$

$$R^{\pm} \xrightarrow{k_2} R^{\pm} + X_2^{\pm}, X_2^{\pm} \xrightarrow{k_3} \phi, X_2^{+} + X_2^{-} \xrightarrow{ann} \phi \tag{60}$$

$$X_1^{\pm} \xrightarrow{cat} X_1^{\pm} + V^{\pm}, X_2^{\pm} \xrightarrow{cat} X_2^{\pm} + V^{\pm}, V^{\pm} \xrightarrow{deg} \phi, V^{+} + V^{-} \xrightarrow{ann} \phi \tag{61}$$

$$V^{\pm} \xrightarrow{cat} V^{\pm} + E^{\pm}, Y^{\pm} \xrightarrow{cat} Y^{\pm} + E^{\mp}, E^{\pm} \xrightarrow{deg} \phi, E^{+} + E^{-} \xrightarrow{ann} \phi \tag{62}$$

$$E^{\pm} \xrightarrow{k_4} E^{\pm} + X_3^{\pm}, X_3^{\pm} \xrightarrow{deg} \phi, X_3^{+} + X_3^{-} \xrightarrow{ann} \phi \tag{63}$$

$$E^{\pm} \xrightarrow{k_5} E^{\pm} + X_4^{\pm}, X_4^{+} + X_4^{-} \xrightarrow{ann} \phi, X_4^{\pm} \xrightarrow{cat} X_4^{\pm} + M^{\pm} \tag{64}$$

$$E^{\pm} \xrightarrow{k_6} E^{\pm} + X_5^{\pm}, X_5^{\pm} \xrightarrow{k_7} \phi, X_5^{+} + X_5^{-} \xrightarrow{ann} \phi \tag{65}$$

$$X_3^{\pm} \xrightarrow{cat} X_3^{\pm} + M^{\pm}, X_5^{\pm} \xrightarrow{cat} X_5^{\pm} + M^{\mp}, M^{\pm} \xrightarrow{deg} \phi, M^{+} + M^{-} \xrightarrow{ann} \phi \tag{66}$$

The controller $C_1(s)$ shown in Fig. 13 is established by (59)-(61). The controller $C_2(s)$ shown in Fig. 14 is established by (63)-(66). The tracking error signal $e = v - y$ is generated by (62). The integral element $x_1 = k_1 r$ and the differential element x'' are expressed in (59)-(60). The summing process of x_1 and x_2 is expressed by (61). The integral element

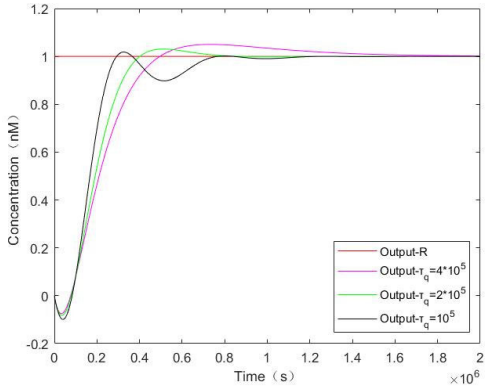

FIGURE 17. Step response curve of MDOB-PID based on CRNs when $r(t) = 1(t), d(t) = 0(t)$.

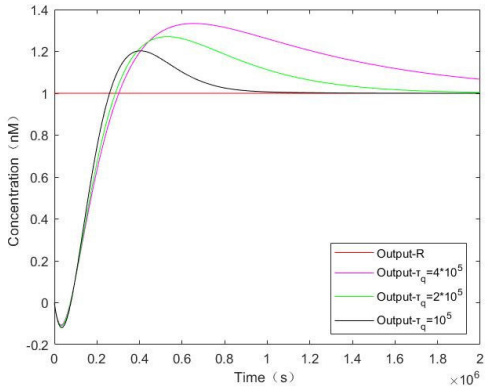

FIGURE 18. Step response curve of MDOB-PID based on CRNs when $r(t) = 1(t), d(t) = 2(t)$.

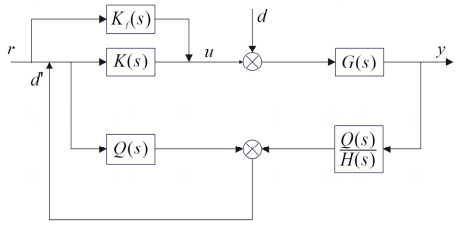

FIGURE 19. Structure of FDOB-PID control system.

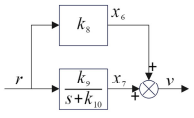

FIGURE 20. The relationship among the reactant species used to implement the controller $K_f(s)$.

$x_3 = k_4 e$, the integral element $x_4 = k_5 e$, and the differential element $x_5 = k_6 x_3 + k_7 e$, are expressed in (63)-(65). The summing process of x_3, x_4, and x_5 is expressed by (66). Visual depiction of (59)-(66) is shown in Fig. **15**.

The kinetic equations of the reactant species used to implement the MDOB-PID in (59)-(66) can be represented by the

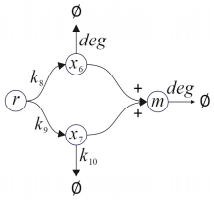

FIGURE 21. Visual depiction of CRNs for $K_f(s)$ (77)-(79).

following equations:

$$\dot{x}_1^{\pm} = k_1 * r^{\pm} - deg * x_1^{\pm} - ann * x_1^{+} x_1^{-} \tag{67}$$
$$\dot{x}_2^{\pm} = k_2 * e^{\pm} - k_3 * x_2^{\pm} - ann * x_2^{+} x_2^{-} \tag{68}$$
$$\dot{e}^{\pm} = cat * v^{\pm} + deg * y^{\mp} - deg * e^{\pm} - ann * e^{+} e^{-} \tag{69}$$
$$\dot{x}_3^{\pm} = k_4 * e^{\pm} - deg * x_3^{\pm} - ann * x_3^{+} x_3^{-} \tag{70}$$
$$\dot{x}_4^{\pm} = k_5 * e^{\pm} - ann * x_4^{+} x_4^{-} \tag{71}$$
$$\dot{x}_5^{\pm} = k_6 * e^{\pm} - k_7 * x_5^{\pm} - ann * x_5^{+} x_5^{-} \tag{72}$$

Remark 8: The CRNs used to implement MDOB-PID are presented in this part. By utilizing the CRNs (59)-(66) provided in this subsection, it is possible to carry out the simulation of the CRNs-based MDOB-PID control system. Then, according to the transfer function (49)-(50), it can be found that there are two kinds of control characteristic coupling problems in the existing improvement scheme, and the existing problems will be further explained through simulation.

C. SIMULATION OF CRNS-BASED MDOB-PID CONTROL SYSTEM

In this subsection, the validity of the MDOB-PID control system described in (59)-(66) is confirmed through the simulation.

The parameters of the controlled object $G_p(s)$ of (41) are listed in Table **5**. Similarly, the FDA is used to tune the two parameters (τ_q and τ_c) in the MDOB-PID of (59)-(66).

The parameter optimization process of MDOB-PID and the step response after optimization are shown in Fig. **16**. According to the optimization results of the FDA, the optimal control system parameters can be obtained as $\tau_q = 2 \times 10^5$ and $\tau_c = 2 \times 10^5$. To verify the issue of coupling between the two features of MDOB-PID, the parameter τ_c is kept constant while enlarging the value of τ_q to 4×10^5 and reducing the value of τ_q to 10^5, respectively, after which their step response performance will be compared. The reaction rates of CRNs shown in Table **6** can be obtained by (57)-(58).

Through Visual DSD for simulation, the step response curves for MDOB-PID are shown in Fig. **17** and Fig. **18**, where Output-$\tau_q = 4 \times 10^5$, Output-$\tau_q = 2 \times 10^5$, and Output-$\tau_q = 10^5$ represent the step response of MDOB-PID under different parameters, respectively.

As shown in Fig. **17** and Fig. **18**, when there is no disturbance in the MDOB-PID control system, a lower value of τ_q leads to a more rapid step response, that is, the smaller rise

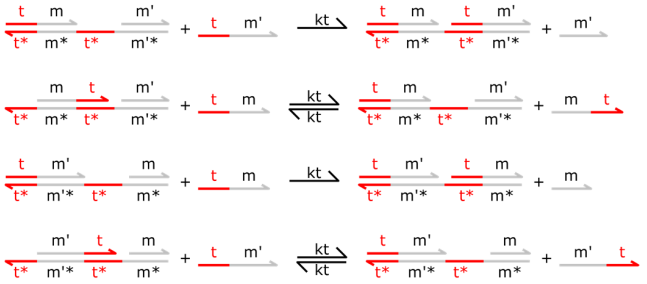

FIGURE 22. Schematic diagram of a DNA molecule for annihilation reaction $M^+ + M^- \xrightarrow{k} \phi$.

TABLE 9. Parameters of the MDOB-PID and FDOB-PID based on CRNs.

MDOB-PID	FDOB-PID
$k_1 = 0.5$	$k_1 = 0.5$
$k_2 = 0.0000025$	$k_2 = 0.0000025$
$k_3 = 0.000005$	$k_3 = 0.000005$
$k_4 = 2$	$k_4 = 2$
$k_5 = 0.00001$	$k_5 = 0.00001$
	$k_6 = 2.0025$
	$k_7 = 0.00004$
	$k_8 = 0.00002$

time and the smaller overshoot. When there is disturbance $d(t) = 1(t)$ in the system, the smaller the τ_q is, the stronger the disturbance suppression effect will be. At the same time, it is also found that when $\tau_q < \tau_c$ the system step response will produce a certain oscillation and the settling time will become longer. It means that when lowering the value of τ_q to obtain the stronger disturbance suppression effect, its set-point tracking will be weakened, in other words, the current MDOB-PID control system couples the disturbance suppression characteristic with the setpoint tracking characteristic. A compromise between the two parameters is required. The respective data in detail are displayed in Table 7 and Table 8.

Remark 9: A simulation comparison of the CRNs-based MDOB-PID under different parameter conditions is provided. It is demonstrated that the MDOB-PID control system is capable of overcoming its reliance on the inverse nominal model. At the same time, it is also found that there are still some problems in the MDOB-PID control system, such as the coupling of two control characteristics. To solve this problem, the solution is given in the next paragraph of this paper, namely, combining the feed-forward controller with the MDOB-PID controller system to achieve decoupling of the control characteristics.

IV. FDOB PID CONTROL SYSTEM

A. DESIGN IDEAL

According to the two transfer functions (49)(50) of the MDOB-PID control system, it discovers that both of them include filters $Q(s)$ and $H(s)$, which indicates that its setting

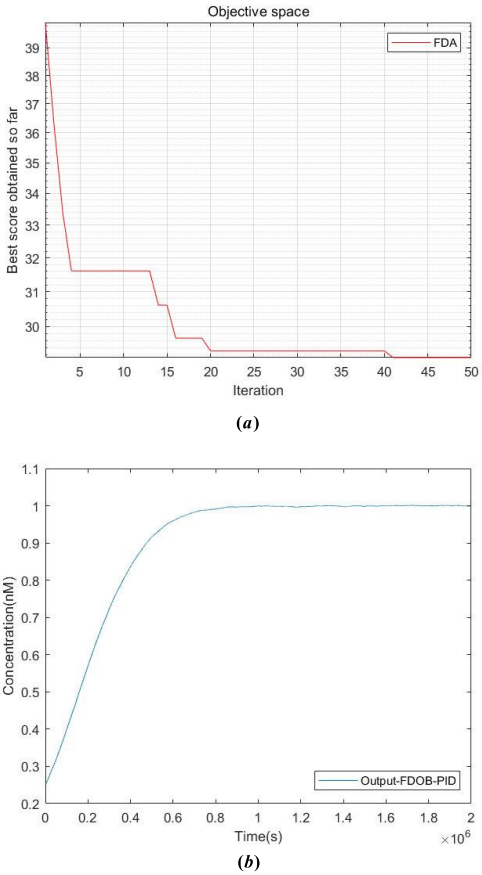

FIGURE 23. (*a*) The process of tuning controller parameters in FDOB-PID by FDA (*b*) Step response of FDOB-PID control system.

TABLE 10. Step response performance of FDOB-PID based on CRNs, when $r(t) = 1(t)$, $d(t) = 0(t)$.

Control system	$r(t) = 1(t)$, $d(t) = 0(t)$		
	Rise time	Settling time	Overshoot
MDOB-PID	246179s	695519s	1.80%
FDOB-PID	450162s	**544497s**	**0%**

point tracking characteristics and disturbance suppression characteristics have not been decoupled, meaning that τ_q and τ_c can only be set to make a compromise between the setting point tracking characteristic and the disturbance suppression characteristic. In order to decouple the two characteristics, a feedforward controller is added to the control system, and the block diagram is shown in Fig. 19.

With reference to Fig. 19, two transfer functions of close-loop can be obtained as follows:

$$G_{ry} = \frac{G(s)H(s)K(s) + G(s)K_f(s)[1 - Q(s)]}{H(s)[1 - Q(s)] + G(s)Q(s)K(s)} \tag{73}$$

$$G_{dy} = \frac{G(s)H(s)[1 - Q(s)]}{H(s)[1 - Q(s)] + G(s)Q(s)K(s)} \tag{74}$$

where (73) is from input signal r to output signal y and (74) is from disturbance signal d to output signal y. While

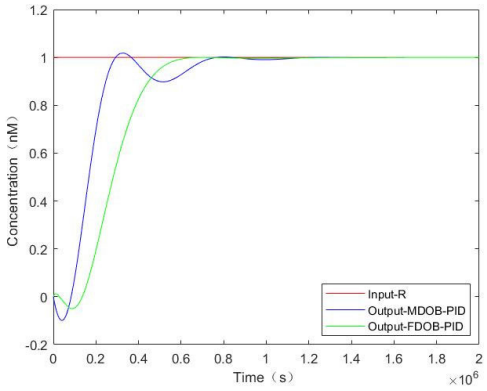

FIGURE 24. Step response curve of FDOB-PID based on CRNs, when $r(t) = 1(t), d(t) = 0(t)$.

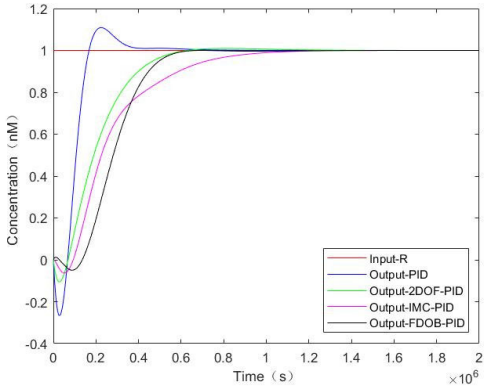

FIGURE 25. Step response curve of different control system based on CRNs when $r(t) = 1(t), d(t) = 0(t)$.

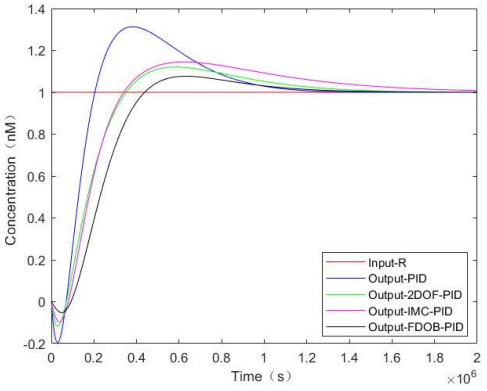

FIGURE 26. Step response curve of different control system based on CRNs when $r(t) = 1(t), d(t) = 2(t)$.

feedforward controller $K_f(s)$ has the following form

$$K_f(s) = -(\alpha + \beta s) \tag{75}$$

where α and β are parameters of feedforward controller.

According to Fig. **19** and two transfer functions (73)(74), evidently, the FDOB-PID control system is capable of realizing the decoupling of set-point tracking characteristic and disturbance suppression characteristic without relying on

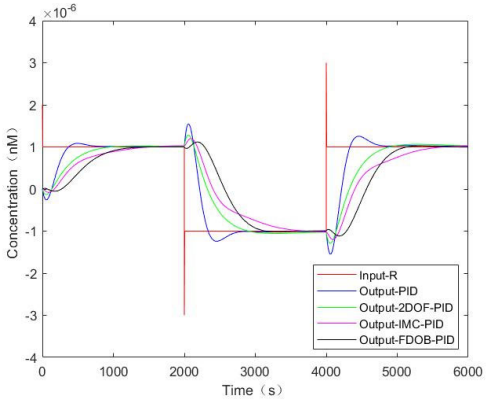

FIGURE 27. Step response curve of different control system based on DSD when $r(t) = 1(t), d(t) = 0(t)$.

the inverse nominal model. The design idea is to realize disturbance suppression by designing disturbance observer parameters τ_q and τ_c, and then designing feedforward parameters to realize set-point tracking.

B. CRNS-BASED FDOB-PID CONTROL SYSTEM

In order to make $K_f(s)$ more suitable for the implementation of CRNs, it is approximated as follow:

$$K_f(s) = -(\alpha + \beta s) = k_8 - \frac{k_9}{s + k_{10}} \tag{76}$$

The control structure of the controllers $K_f(s)$ can be determined from (76) and is seen in Fig. **20**, whose CRNs are as follows:

$$R^{\pm} \xrightarrow{k_8} R^{\pm} + X_6^{\pm}, X_6^{\pm} \xrightarrow{ann} \phi, X_6^{+} + X_6^{-} \xrightarrow{deg} \phi \tag{77}$$

$$R^{\pm} \xrightarrow{k_9} E^{\pm} + X_7^{\pm}, X_7^{\pm} \xrightarrow{k_{10}} \phi, X_7^{+} + X_7^{-} \xrightarrow{deg} \phi \tag{78}$$

$$X_6^{\pm} \xrightarrow{cat} X_6^{\pm} + M^{\mp}, X_7^{\pm} \xrightarrow{cat} X_7^{\pm} + M^{\pm}, M^{\pm} \xrightarrow{deg} \phi, M^{-} \xrightarrow{deg} \phi \tag{79}$$

The controller $K_f(s)$ shown in Fig. **20** is established by (77)-(79). The integral element $x_6 = k_8 e$ and the integral element $x_7 = k_{10} x_3 + k_9 e$ are expressed in (77)-(78). The summing process of x_6 and x_7 is expressed by (78). The FDOB-PID based on CRNs can be formed by (59)-(66) and (77)-(79). Visual depiction of (77)-(79) is shown in Fig. **21**.

Remark 10: In this section, aiming at the coupling problem of set-point tracking and disturbance suppression existing in MDOB-PID, the design idea of FDOB-PID control system design is given. FDOB-PID realizes the decoupling of two characteristics, and the parameter design is freer and more convenient. Then, the CRNs for realizing FDOB-PID are given. The simulation of the FDOB-PID control system can be completed by (59)-(66) and (77)-(79) given in this section.

C. FDOB-PID CONTROL SYSTEM BASED ON DSD

The DSD reaction utilizes the replaced single strand for signal transmission in DNA computing processes, effectively solving the issue of signal transmission in DNA computing.

TABLE 11. Step response performance of different control system based on CRNs, when $r(t) = 1(t)$, $d(t) = 0(t)$.

Control system	$r(t) = 1(t),\ d(t) = 0(t)$		
	Rise time	Settling time	Overshoot
PID[16]	152634s	352540s	10.88%
2DOF-PID[17]	410777s	538101s	0.93%
IMC-PID[28]	587737s	892306s	0.012%
FDOB-PID	450162s	544497s	**0%**

TABLE 12. Step response performance of different control system based on CRNs, when $r(t) = 1(t)$, $d(t) = 2(t)$.

Control system	$r(t) = 1(t),\ d(t) = 2(t)$		
	Rise time	Settling time	Overshoot
PID[16]	184370s	1065103s	31.11%
2DOF-PID[17]	296554s	1284104s	12.06%
IMC-PID[28]	290709s	1676152s	14.4%
FDOB-PID	362749s	**1124415s**	**7.6%**

TABLE 13. Step response curve of different control system based on DSD, when $r(t) = 1(t)$, $d(t) = 0(t)$.

Control system	$r(t) = 1(t),\ d(t) = 0(t)$		
	Overshoot_1	Overshoot_2	Overshoot_3
PID[16]	8.55%	23.68%	25.46%
2DOF-PID[17]	2.37%	5.48%	6.26%
IMC-PID[28]	0.87%	2.24%	3.15%
FDOB-PID	**0.11%**	**2.11%**	**2.52%**

As a result, the DSD reaction enables the construction of logic gates, as well as more intricate molecular controllers and arithmetic gates, using DNA molecules. Meanwhile, DNA molecules are considered to be one of the ideal materials for constructing CRNs. Catalysis reactions, annihilation reactions, and degradation reactions in CRNs can be performed using DSD reaction network modules. For example, an annihilation reaction in CRNs of (66) is $M^+ + M^- \xrightarrow{k} \phi$,which can be converted into DSD as follows:

$$sp1 + M' \xrightarrow{k} sp5 + sp6 \tag{80}$$

$$Ann1 + M \overset{k}{\Leftrightarrow} sp1 + Ann3 \tag{81}$$

$$sp2 + M \xrightarrow{k} sp3 + sp4 \tag{82}$$

$$Ann2 + M' \overset{k}{\Leftrightarrow} sp2 + Ann4 \tag{83}$$

where $Ann1$, $Ann2$, $Ann3$,and $Ann4$ are auxiliary substrates. Their initial concentration is chosen to be $Cmax = 1000nm$ to ensure that they fully react with the input chemicals. M and M' represent the reactants M^+ and M^- in the annihilation reaction. $sp1$, $sp2$, $sp3$, $sp4$, $sp5$, and $sp6$ are all intermediate products.

A schematic diagram of the DNA molecule of the annihilation reaction $M^+ + M^- \xrightarrow{k} \phi$ in (66) is shown in Fig. **21**. The reactants and products in (80)-(81) can be mapped to the DNA molecule in Fig. **22**. According to (80) and (81), the toehold t in the single-stranded M^+ and the toehold t^* in the auxiliary substrate $Ann1$ undergo DSD reaction based on the principle of complementary base pairing. Subsequently, domain m undergoes branch migration, resulting in the formation of the auxiliary substrate $Ann2$ and intermediate $sp1$. Afterwards, intermediate $sp1$ further undergoes DSD reactions with single-stranded M^- following the principle of base complementary pairing, leading to the generation of the released substances $sp5$ and $sp6$. Simultaneously, (82) and (83) also undergo the aforementioned reactions until the annihilation of the initial substrates M^+ and M^-. By realizing the catalytic reaction, degradation reaction, and annihilation reaction of CRNs in the DSD reaction network, a firm groundwork has been established to actualize FDOB-PID within the DSD reaction network.

D. SIMULATION OF CRNS-BASED AND DSD-BASED FDOB-PID CONTROL SYSTEM

The simulation between MDOB-PID of (59)-(66), and the FDOB-PID of (59)-(66) with (77)-(79) is given in this subsection. The controlled object $G_p(s)$f (41) are listed in Table **5**.

Similarly, the FDA is used to tune the four parameters (τ_q, τ_c, α,and β) in the FDOB-PID of (59)-(66) with (77)-(79).

The parameter optimization process of FDOB-PID and the step response after optimization are shown in Fig. **23**. According to the optimization results of the FDA, the optimal control system parameters can be obtained as $\tau_q = 2 \times 10^5$, $\tau_c = 2 \times 10^5$, $\alpha = 0.025$, and $\beta = 1 \times 10^5$. The reaction rates of CRNs shown in Table **9** can be obtained by (57)- (58) with (76).

The step response curves for MDOB-PID and FDOB-PID are obtained from Visual DSD as shown in Fig. **24**, where Output-MDOB-PID represents the step response of MDOB-PID and Output-FDOB-PID represents the step response of FDOB-PID.

As shown in Fig. **24**, when there is no external disturbance in the system, although the rise time of the step response becomes larger after adding a feedforward controller, it reduces the oscillation of the control system and the overshoot is almost 0, the settling time of the step response becomes shorter, and the system tends to a stable state faster. The FDOB-PID control system can adjust its ability to suppress disturbances by altering the values of τ_q and τ_c. Additionally, the parameters α and β can be adjusted to modify the setpoint tracking capabilities of the FDOB-PID control system, and there is no need to choose parameters between the two characteristics. Smaller overshoot and a better disturbance suppression effect can be accomplished through parameter adjustment, and the control system goes to a stable state more quickly. The data in detail are displayed in Table **10**.

For the purpose of proving the superiority of the FDOB-PID control system even more, the PID [16], the 2DOF-PID [17], and the IMC-PID [28] are selected as the comparison objects.

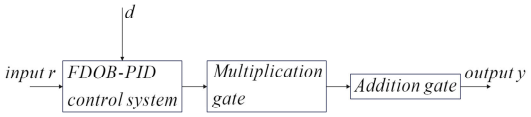

FIGURE 28. Structure of the exponential gate control system.

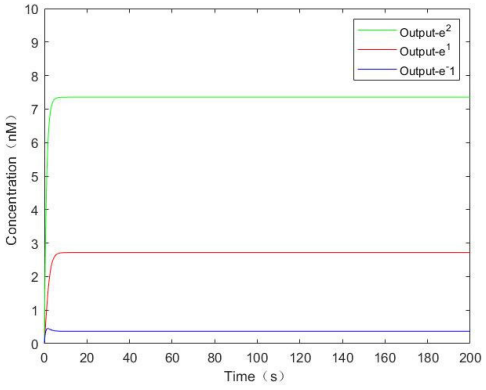

(*a*)

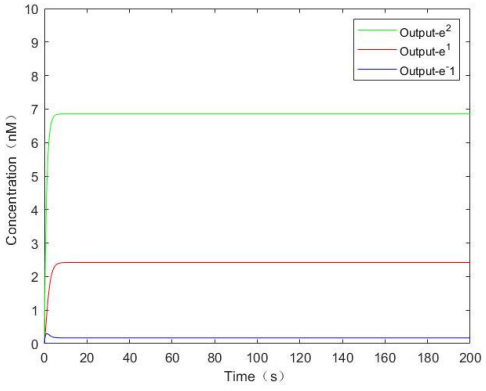

(*b*)

FIGURE 29. Calculation results of exponential gate (*a*) when there is no leak reaction (*b*) when the initial species *x* leak.

The controlled objects are $G_p(s)$ of (41) listed in Table **5**. The step response can be obtained as shown in Fig. **25** and Fig. **26**.

The step response curves for PID [16], 2DOF-PID [17], IMC-PID [28], and FDOB-PID are accepted from Visual DSD as shown in Fig. **25** and Fig. **26**,where Output-PID represents the step response of PID [16], Output-2DOF PID represents the step response of 2DOF PID [17], Output-IMC PID represents the step response of IMC PID [28], and Output-FDOB-PID represents the step response of FDOB-PID.

As can be seen in Fig. **25** and Fig. **26**, PID [16], 2DOF-PID [17], IMC-PID [28], and the FDOB-PID in this paper are compared. When there is no external disturbance in the system, the step response overshoot of the FDOB-PID in this paper is 0%, which is significantly lower than the PID [16], 2DOF-PID [17], and IMC-PID [28]. When there is an external disturbance $d(t) = 2(t)$, the disturbance suppression effect of the FDOB-PID is stronger than that of PID [16],

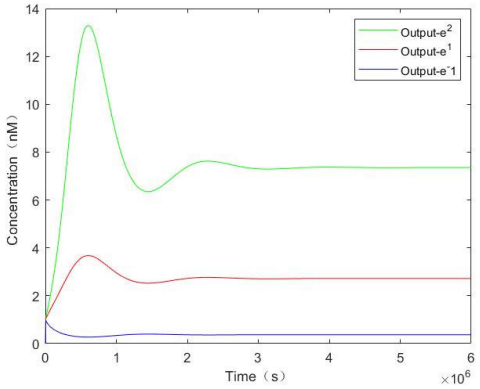

FIGURE 30. Calculation results of exponential gate control system with leak reaction.

2DOF-PID [17], and IMC-PID [28], the step response curve is smoother, and the settling time is 1124415s. At the same time, the overshoot of FDOB-PID is 7.6%, which is smaller than the 2DOF-PID [17] and IMC-PID [28]. Although the settling time of PID [16] can be shorter, its overshoot has a value of 31.11%, which is much larger than the control system in this paper. Detailed information on the specific data is presented in Table **11** and Table **12**. In summary, the simulation results indicate that the FDOB-PID based on CRNs has certain advantages in terms of overshoot and settling time.

It is well known that DSD has the capability of implementing three fundamental reaction modules, namely, catalytic reaction, annihilation reaction, and degradation reaction, in CRNs. The CRNs in (42)-(44), (59)-(66), and (77)-(79) are composed of these three reaction modules. Next, this paper realizes the DSD-based FDOB-PID by mapping the abstract CRNs to DSD.

The step responses of PID [16], 2DOF-PID [17], IMC-PID [28], and the FDOB-PD based on the DSD reaction networks are given in Fig. **27**.

As shown in Fig. **27** and Table **13**, all four control systems can correctly track the setpoint, but three times overshoots of the FDOB-PID are 0.11%, 2.11%, and 2.52%, respectively, which are smaller than the overshoots of the other three control systems.

Remark 11: In this part, several simulations and comparisons between the FDOB-PID control system and other molecular control systems are provided. As shown in Fig. **25**-Fig. **27** and Table **11** - Table **13**, the FDOB-PID control system is superior to other molecular controllers in terms of overshoot and settling time.

V. ESTABLISHING AN EXPONENTIAL GATE CONTROL SYSTEM TO SUPPRESS LEAKY REACTION

The DSD reaction enables the construction of molecular arithmetic gates using DNA molecules which are essential components of DNA computing. Meanwhile, the most typical use of biological controllers in applications is to restrain leak reactions in operational gates. In this subsection, an expo-

nential gate is constructed by DSD, where the leak reaction is treated as a disturbance. Then the FDOB-PID is used to restrain the impact of the leak reaction. Since there is no ready-made exponential operation method in CRNs, it uses the series expansion method to expand and sum the exponential operation, and finally get the result of the exponential operation, that is, convert the exponential operation into addition and multiplication.

$$e^x = 1 + x + \frac{1}{2!}x^2 + \frac{1}{3!}x^3 + o\left(x^3\right) \tag{84}$$

The exponential gate can be built by CRNs as follows:

$$R^{\pm} \xrightarrow{K} B^{\pm}, A^{\pm} \xrightarrow{K_1} B^{\pm}, 2A^{\pm} \xrightarrow{K_2} B^{\pm} \tag{85}$$

$$3A^{\pm} \xrightarrow{K_3} B^{\pm}, 4A^{\pm} \xrightarrow{K_4} B^{\pm}, 5A^{\pm} \xrightarrow{K_5} B^{\pm} \tag{86}$$

$$A^{\pm} \xrightarrow{\gamma} \phi \tag{87}$$

where $R^{\pm}$ represents the constant initial value concentration, $A^{\pm}$ represents the initial concentration of exponent x, $B^{\pm}$ represents the concentration of e^x after exponential operation, K_n represents the reaction rate. In order to make the approximate result closer to the exact value, (84) is expanded to the fifth term. The exponential gate control system is established by combining a FDOB-PID control system, a multiplication gate, and an accumulator, as shown in Fig. **28**.

e^1, e^2, and e^{-1} are selected to verify the effectiveness of the exponential operation gate. As shown in Fig. **29(a)**, when there is no leak reaction, the calculation results are 2.718, 7.355, and 0.368, which prove that the exponential operation gate can obtain accurate calculation outcomes. However, if a leak reaction occurs, since the input value x of the exponential operation gate can be multiplied and added to obtain the output, even a small leak reaction can cause calculation errors. According to Fig. **29(b)**, the calculation results are 2.413, 6.855, and 0.167, respectively.

For the sake of suppressing the impact of leak reaction on calculation outcomes, the FDOB-PID is used to establish an exponential operation control system, as shown in Fig. **28**.

The output curve of the exponential operation control system with a leak reaction can be seen in Fig. **30**. It can be observed that the final results e^1, e^2, and e^{-1} are 2.718, 7.355, and 0.368, respectively. Therefore, the FDOB-PID control system is capable of efficiently suppressing the impact of leak reaction, thereby ensuring accurate computation outcomes.

Remark 12: In this section, FDOB-PID and molecular exponential gates are utilized to construct an exponential gate control system, as depicted in Fig. **28**. The simulation results, presented in Fig. **30**, demonstrate that FDOB-PID can effectively suppress the influence of leak reactions in exponential gates on calculation outcomes.

VI. CONCLUSION

The DOB-PID control system is established using CRNs and DSD in this paper. The primary aim of this system is suppressing the impact of leak reactions on the exponential gate. First, a DOB-PID control system is established by CRNs, whose parameters are tuned by flow direction optimization algorithm. The derivation of transfer function and simulation results indicate that the DOB-PID control system exhibits a superior ability to suppress disturbances. Then, the structure of the disturbance observer is improved, leading to the establishment of a MDOB-PID control system via CRNs, which overcomes the limitation that the classical disturbance observer depends on the plant model. Afterwards, combining feedforward controller and disturbance observer, a FDOB-PID control system is established using CRNs and DSD. It proves that the FDOB-PID control system, which has a stronger disturbance suppression effect and a lower overshoot, can realize the decoupling of the disturbance suppression characteristic and the setpoint tracking characteristic. Finally, for the sake of suppressing the impact of the leak reactions, an exponential gate control system is established. Based on the simulation outcomes, it is permissible to draw the conclusion that the FDOB-PID control system is capable of efficiently suppressing the impact of leak reactions and obtain correct calculation results. More attention will be paid to combining control theory with biochemistry to explore more effective methods to suppress the leak reaction in biochemical processes in future.

REFERENCES

[1] S. M. Brooks and H. S. Alper, "Applications, challenges, and needs for employing synthetic biology beyond the lab," *Nature Commun.*, vol. 12, no. 1, Mar. 2021, Art. no. 1390.
[2] D. Sharma and M. Ramteke, "DNA computing: Methodologies and challenges," in *DNA- and RNA-Based Computing Systems*. Weinheim, Germany: Wiley-VCH, 2021, pp. 15–29, doi: 10.1002/9783527825424.
[3] S. Zhao, L. Yu, S. Yang, X. Tang, K. Chang, and M. Chen, "Boolean logic gate based on DNA strand displacement for biosensing: Current and emerging strategies," *Nanosc. Horizons*, vol. 6, no. 4, pp. 298–310, Apr. 2021.
[4] E. Zhu, C. Chen, Y. Rao, and W. Xiong, "Biochemical logic circuits based on DNA combinatorial displacement," *IEEE Access*, vol. 8, pp. 34096–34103, 2020.
[5] P. A. C. Oliveira, J. V. C. Teixeira, R. A. Marks, M. V. Guterres, and O. P. V. Neto, "Evaluating analog arithmetic circuit for approximate computing with DNA strand displacement," *Anal. Integr. Circuits Signal Process.*, vol. 108, no. 3, pp. 485–493, Sep. 2021.
[6] Y. A. Khan, K. I. White, and A. T. Brunger, "The AAA+ superfamily: A review of the structural and mechanistic principles of these molecular machines," *Crit. Rev. Biochemistry Mol. Biol.*, vol. 57, no. 2, pp. 156–187, Oct. 2022.
[7] P. Zhang, J. Jiang, R. Yuan, Y. Zhuo, and Y. Chai, "Highly ordered and field-free 3D DNA nanostructure: The next generation of DNA nanomachine for rapid single-step sensing," *J. Amer. Chem. Soc.*, vol. 140, no. 30, pp. 9361–9364, Jul. 2018.
[8] X. Zhang, Q. Zhang, Y. Liu, B. Wang, and S. Zhou, "A molecular device: A DNA molecular lock driven by the nicking enzymes," *Comput. Struct. Biotechnol. J.*, vol. 18, pp. 2107–2116, Jan. 2020.
[9] M. Feinberg, *Foundations of Chemical Reaction Network Theory*, vol. 202. Cham, Switzerland: Springer, 2019, doi: 10.1007/978-3-030-03858-8.
[10] P. Schwaller, T. Laino, T. Gaudin, P. Bolgar, C. A. Hunter, C. Bekas, and A. A. Lee, "Molecular transformer: A model for uncertainty-calibrated chemical reaction prediction," *ACS Central Sci.*, vol. 5, no. 9, pp. 1572–1583, Aug. 2019.
[11] D. Fan, J. Wang, E. Wang, and S. Dong, "Propelling DNA computing with materials' power: Recent advancements in innovative DNA logic computing systems and smart bio-applications," *Adv. Sci.*, vol. 7, no. 24, Dec. 2020, Art. no. 2001766.
[12] H. Lv, Q. Li, J. Shi, C. Fan, and F. Wang, "Biocomputing based on DNA strand displacement reactions," *ChemPhysChem*, vol. 22, no. 12, pp. 1151–1166, Jun. 2021.

[13] C. Chen, J. Wen, Z. Wen, S. Song, and X. Shi, "DNA strand displacement based computational systems and their applications," *Frontiers Genet.*, vol. 14, Feb. 2023, Art. no. 1120791.
[14] B. Yordanov, J. Kim, R. L. Petersen, A. Shudy, V. V. Kulkarni, and A. Phillips, "Computational design of nucleic acid feedback control circuits," *ACS Synth. Biol.*, vol. 3, no. 8, pp. 600–616, Aug. 2014.
[15] R. Sawlekar, F. Montefusco, V. V. Kulkarni, and D. G. Bates, "Implementing nonlinear feedback controllers using DNA strand displacement reactions," *IEEE Trans. Nanobiosci.*, vol. 15, no. 5, pp. 443–454, Jul. 2016.
[16] N. M. G. Paulino, M. Foo, J. Kim, and D. G. Bates, "PID and state feedback controllers using DNA strand displacement reactions," *IEEE Control Syst. Lett.*, vol. 3, no. 4, pp. 805–810, Oct. 2019.
[17] Y. Yuan, H. Lv, and Q. Zhang, "DNA strand displacement reactions to accomplish a two-degree-of-freedom PID controller and its application in subtraction gate," *IEEE Trans. Nanobiosci.*, vol. 20, no. 4, pp. 554–564, Oct. 2021.
[18] H. Xue, H. Lv, Y. Xiao, and X. Wang, "Cascade PID control systems based on DNA strand displacement with application in polarization of tumor-associated macrophages," *IEEE Access*, vol. 11, pp. 38563–38577, 2023.
[19] E. Satir and O. Kendirli, "A symmetric DNA encryption process with a biotechnical hardware," *J. King Saud Univ.-Sci.*, vol. 34, no. 3, Apr. 2022, Art. no. 101838.
[20] J. Gao and T. Xie, "DNA computing in cryptography," *Adv. Comput.*, vol. 129, pp. 83–128, Feb. 2023.
[21] K. Tarun and N. Suyel, "Introduction to DNA computing," *Adv. Comput.*, vol. 129, pp. 1–38, Feb. 2023.
[22] Y. Wang, T. Mao, J. Sun, and P. Liu, "Exponential function computation based on DNA strand displacement circuits," *IEEE Trans. Biomed. Circuits Syst.*, vol. 16, no. 3, pp. 479–488, Jun. 2022.
[23] J. Sun, C. Sun, Z. Wang, and Y. Wang, "Biosignals secure communication scheme with filtering of active control projection synchronization of biological chaotic circuits with different orders based on DNA strand displacement," *IEEE Trans. Biomed. Circuits Syst.*, vol. 17, no. 3, pp. 1–12, Apr. 2023.
[24] J. Sun, Z. Shan, P. Liu, and Y. Wang, "Backstepping synchronization control for three-dimensional chaotic oscillatory system via DNA strand displacement," *IEEE Trans. Nanobiosci.*, vol. 22, no. 3, pp. 511–522, Jul. 2023.
[25] T. Song, S. Garg, R. Mokhtar, H. Bui, and J. Reif, "Analog computation by DNA strand displacement circuits," *ACS Synth. Biol.*, vol. 5, no. 8, pp. 898–912, Jul. 2016.
[26] Y. Yuan, H. Lv, and Q. Zhang, "Molecular device design based on chemical reaction networks: State feedback controller, static pre-filter, addition gate control system and full-dimensional state observer," *J. Math. Chem.*, vol. 60, no. 5, pp. 915–935, May 2022.
[27] K. Oishi and E. Klavins, "Biomolecular implementation of linear I/O systems," *IET Syst. Biol.*, vol. 5, no. 4, pp. 252–260, Jul. 2011.
[28] Y. Li, H. Lv, and X. Wang, "The design of 2DOF IMC-PID controller in biochemical reaction networks," *Appl. Sci.*, vol. 13, no. 6, p. 3402, 2023.
[29] A. Bayrak and M. Ö. Efe, "A frequency domain comparison of disturbance observer based control schemes," *Proc. Inst. Mech. Eng., I, J. Syst. Control Eng.*, vol. 236, no. 2, pp. 244–256, Aug. 2022.
[30] J. R. S. Benevides, M. A. D. Paiva, P. V. G. Simplício, R. S. Inoue, and M. H. Terra, "Disturbance observer-based robust control of a quadrotor subject to parametric uncertainties and wind disturbance," *IEEE Access*, vol. 10, pp. 7554–7565, 2022.
[31] X. Meng, H. Yu, J. Zhang, T. Xu, H. Wu, and K. Yan, "Disturbance observer-based feedback linearization control for a quadruple-tank liquid level system," *ISA Trans.*, vol. 122, pp. 146–162, Mar. 2022.
[32] O. Mofid, M. Momeni, S. Mobayen, and A. Fekih, "A disturbance-observer-based sliding mode control for the robust synchronization of uncertain delayed chaotic systems: Application to data security," *IEEE Access*, vol. 9, pp. 16546–16555, 2021.
[33] B. Sarsembayev, K. Suleimenov, and T. D. Do, "High order disturbance observer based PI-PI control system with tracking anti-windup technique for improvement of transient performance of PMSM," *IEEE Access*, vol. 9, pp. 66323–66334, 2021.
[34] H. Karami, M. V. Anaraki, S. Farzin, and S. Mirjalili, "Flow direction algorithm (FDA): A novel optimization approach for solving optimization problems," *Comput. Ind. Eng.*, vol. 156, Jun. 2021, Art. no. 107224.
[35] Y. Fan, S. Zhang, Y. Wang, D. Xu, and Q. Zhang, "An improved flow direction algorithm for engineering optimization problems," *Mathematics*, vol. 11, no. 9, p. 2217, May 2023, Art. no. 2217.
[36] M. H. Zafar, N. M. Khan, M. Mansoor, and U. A. Khan, "Towards green energy for sustainable development: Machine learning based MPPT approach for thermoelectric generator," *J. Cleaner Prod.*, vol. 351, Jun. 2022, Art. no. 131591.

WUJIE ZHANG received the B.E. degree in software engineering from the Nanjing Jincheng College, in 2020. He is currently pursuing the master's degree in software engineering with Dalian University. His research interests include DNA strand displacement, chemical reaction networks, and synthetic control.

HUI LV received the B.S. and M.S. degrees in applied mathematics from Liaoning University, Shenyang, China, in 2004 and 2009, respectively, and the Ph.D. degree in control theory and control engineering from Northeastern University, Shenyang, in 2015.

She is currently an Associate Professor with the Key Laboratory of Advanced Design and Intelligent Computing, Ministry of Education, Dalian University, Dalian, China. Her research interests include hybrid control systems, DNA computing, and chemical reaction networks.